Computing exact coherent states in channels starting from the laminar profile: A resolvent-based approach

Kevin Rosenberg and Beverley J. McKeon

Phys. Rev. E **100**, 021101 — Published 28 August 2019

DOI: 10.1103/PhysRevE.100.021101

Computing exact coherent states in channels starting from the laminar profile: a resolvent-based approach

Kevin Rosenberg and Beverley J. McKeon
Graduate Aerospace Laboratories, California Institute of Technology

We present an iterative method to compute traveling wave exact coherent states (ECS) in Couette and Poiseuille flows starting from an initial laminar profile. The approach utilizes the resolvent operator for a two-dimensional, three-component streamwise-averaged mean and exploits the underlying physics of the self-sustaining process. A singular value decomposition of the resolvent operator is used to obtain the mode shape for a single streamwise-varying Fourier mode. The self-interaction of the single mode is computed and used to generate an updated mean velocity input to the resolvent operator. The process is repeated until a nearly-neutrally stable mean flow that self-sustains is obtained, as defined by suitable convergence criteria; the results are further verified with direct numerical simulation. The approach requires the specification of only two unknown parameters: the wavespeed and amplitude of the mode. It is demonstrated that within as few as three iterations, the initial one-dimensional laminar field can be transformed to a three-dimensional ECS.

I. INTRODUCTION

Exact coherent states (ECS) are invariant solutions to the Navier-Stokes equations (NSE). ECS in the form of equilibria/traveling waves and periodic orbits have been computed for several of the canonical geometries and exhibit statistical and structural features that closely resemble those observed in fully turbulent flows [1]. State-space representations of these solutions [2–4] show a rich set of dynamics which may further our understanding of transition and the underlying structure of turbulence, as well as inform ways to ultimately control it.

Of particular interest has been the connection between ECS and the self-sustaining process (SSP). The work of [5] demonstrated how a streamwise-constant (but spanwise-varying) shear flow can generate wave disturbances via an instability, and the nonlinear self-interaction of the wave can generate the necessary Reynolds stresses to sustain the streamwise-constant flow and thus complete the SSP. Secondary instability analyses of streamwise-constant vortices and streaks in channels have also been investigated by [6, 7]. [8] further elucidated the underlying mechanisms of the SSP via a high-Reynolds number asymptotic vortex-wave interaction theory; they demonstrated excellent agreement between their theory and numerical solutions, even for moderate Reynolds numbers. Such frameworks provide promise to the continued development of self-consistent models which may be broadly applicable to a wide range of flows [9].

The presence of streamwise-constant structures in fully turbulent flows has motivated the development of low-order models as well. In particular, the decomposition of the flow into a streamwise-averaged two-dimensional, three-component (2D/3C) velocity field and streamwise-varying perturbations has been investigated by numerous authors [10–12]. Notably, it has been found that practical simplifications can be made by restricting the permissible nonlinear interactions among the streamwise-varying modes, termed quasilinear or restricted nonlinear (RNL) models. It was found by only allowing self-interactions to feed back to the 2D/3C mean, and either neglecting the other interactions or modeling them with noise, a flow field with many of the salient features of turbulence could be produced that self-sustains; furthermore, only a small number of streamwise-varying modes were needed to achieve this self-sustaining state [13]. Such ideas have also been extended successfully to the description of ECS in channels by [14, 15].

Herein, we wish to extend this type of framework to resolvent-based approaches. It has been previously demonstrated [16, 17] that resolvent analysis can be useful for providing low-order descriptions of ECS in the context of a 1D mean (streamwise and spanwise averaged). Presently, we will formulate the analogous resolvent operator for a 2D/3C mean at finite Reynolds number and leverage our understanding of the underlying self-sustaining mechanisms to develop a physics-based methodology for computing ECS. In this respect, our formulation will share many similarities to the work of [8] but without invoking high-Reynolds number asymptotics. Additionally, we will show the streamwise-averaged mean is particularly relevant from a linear stability perspective in terms of predicting relevant frequencies and flow structures, as analogously explored in flows such as cylinder wakes and thermosolutal convection [18, 19]. Despite the increased complexity with the multi-component and multi-dimensional mean field, we will demonstrate this framework can be used to compute ECS from very minimal *a priori* knowledge, namely starting from an initial laminar field.

II. METHODOLOGY

A. Governing equations

We consider the non-dimensional, incompressible NSE for flow in a channel

$$\begin{aligned} &\frac{\partial \mathbf{u}}{\partial t} + \mathbf{u}\cdot\nabla\mathbf{u} = -\nabla p + \frac{1}{Re}\Delta\mathbf{u} \\ &\nabla\cdot\mathbf{u} = 0. \end{aligned} \tag{1}$$

Here, $\mathbf{u}$ is a three-component velocity field $\mathbf{u} = [u(\mathbf{x},t), v(\mathbf{x},t), w(\mathbf{x},t)]^T$ and $p(\mathbf{x},t)$ is the pressure, each a function of three spatial dimensions $\mathbf{x} = (x,y,z)$ and time t. The components of $\mathbf{u}$ and $\mathbf{x}$ are aligned with the streamwise, wall-normal, and spanwise directions respectively. The equations are non-dimensionalized with h, the channel half-height, and the characteristic velocity $u^\dagger$, yielding the corresponding Reynolds number $Re = \frac{u^\dagger h}{\nu}$ where ν is the kinematic viscosity. In the case of Couette flow, $u^\dagger$ is chosen as half the relative velocity of the moving walls. For Poiseuille flow, we focus on the case of a fixed mass flux, denoted as Q, and use the equivalent laminar centerline velocity $u^\dagger = \frac{3Q}{4h}$. We consider a domain periodic in the streamwise and spanwise directions with lengths of L_x and L_z respectively; the wall-normal domain extends from $y = -1$ to $y = 1$. The velocity field is decomposed into the sum of a 2D/3C streamwise-averaged (and time-averaged) mean, assumed known *a priori*, and corresponding fluctuations

$$\mathbf{u}(\mathbf{x},t) = \mathbf{U}(y,z) + \mathbf{u}'(\mathbf{x},t). \tag{2}$$

Substituting equation 2 into equation 1 yields for the fluctuations

$$\begin{aligned} &\frac{\partial \mathbf{u}'}{\partial t} + \mathbf{U}\cdot\nabla\mathbf{u}' + \mathbf{u}'\cdot\nabla\mathbf{U} + \nabla p' - \frac{1}{Re}\Delta\mathbf{u}' = -\mathbf{u}'\cdot\nabla\mathbf{u}' + \langle\mathbf{u}'\cdot\nabla\mathbf{u}'\rangle \\ &\nabla\cdot\mathbf{u}' = 0, \end{aligned} \tag{3}$$

with $\langle\ \rangle$ denoting an average over x and t. We express the fluctuating velocity and pressure fields as Fourier modes in the streamwise direction and in time

$$\begin{bmatrix} \mathbf{u}'(x,y,z,t) \\ p'(x,y,z,t) \end{bmatrix} = \iint_{-\infty}^{\infty} \begin{bmatrix} \hat{\mathbf{u}}(k_x,\omega;y,z) \\ \hat{p}(k_x,\omega;y,z) \end{bmatrix} e^{i(k_x x - \omega t)} \mathrm{d}k_x \mathrm{d}\omega, \tag{4}$$

where we introduce the streamwise wavenumber k_x and temporal frequency ω. We can eliminate the pressure and rewrite the equations for the fluctuations in terms of the vertical velocity $\hat{v}$ and normal vorticity $\hat{\eta} = \hat{u}_z - ik_x\hat{w}$. Following the notation of [12], we define $\Delta = \partial_{yy}^2 + \partial_{zz}^2 - k_x^2$, $\Delta_2 = \partial_{zz}^2 - k_x^2$ and express the governing equations as

$$(-i\omega\boldsymbol{I} + \mathcal{L}_1)\begin{pmatrix} \hat{v} \\ \hat{\eta} \end{pmatrix} = \boldsymbol{B}\hat{\mathbf{f}}, \tag{5}$$

where

$$\mathcal{L}_1 = \boldsymbol{M}^{-1}\mathcal{L}, \tag{6}$$

$$\boldsymbol{M} = \begin{pmatrix} -\Delta & 0 \\ 0 & 1 \end{pmatrix}, \tag{7}$$

$$\mathcal{L} = \begin{pmatrix} \mathcal{L}_{OS} & \mathcal{L}_{C_1} \\ \mathcal{L}_{C_2} & \mathcal{L}_{SQ} \end{pmatrix}, \tag{8}$$

$$\boldsymbol{B} = \boldsymbol{M}^{-1}\begin{pmatrix} -ik_x\partial_y & \Delta_2 & -\partial_{yz}^2 \\ \partial_z & 0 & -ik_x \end{pmatrix}, \tag{9}$$

and $\hat{\mathbf{f}} = \left(\hat{f}_u, \hat{f}_v, \hat{f}_w\right)^T = -\left(\mathbf{u}'\cdot\nabla\mathbf{u}'\right)_{\mathbf{k}}$ is the Fourier-transformed nonlinear forcing term where $\mathbf{k}$ denotes the wavenumber pair (k_x,ω). The full mathematical form of the block operators in $\mathcal{L}$, the linearized Navier-Stokes operator associated with $\mathbf{U}(y,z)$ comprised of Orr-Sommerfeld (OS), Squire (SQ), and coupling (C) operators, is found in the appendix. Equation 5 is recast into the input/output form

$$\hat{\mathbf{u}} = \mathcal{H}(k_x,\omega)\hat{\mathbf{f}}, \tag{10}$$

where the resolvent operator is given by

$$\mathcal{H}(k_x,\omega) = \mathcal{C}(-i\omega \boldsymbol{I} + \mathcal{L}_1)^{-1}\boldsymbol{B}, \tag{11}$$

and

$$\mathcal{C} = \begin{pmatrix} -ik_x{\Delta_2}^{-1}\partial_y & {\Delta_2}^{-1}\partial_z \\ 1 & 0 \\ -{\Delta_2}^{-1}\partial_{yz}^2 & -ik_x{\Delta_2}^{-1} \end{pmatrix}. \tag{12}$$

Notably, $\mathcal{H}(k_x,\omega)$ requires only $\mathbf{U}(y,z)$ as an input. For numerical implementation, the wall-normal operators are discretized with Chebyshev differentiation matrices while Fourier differentiation matrices are used for the operators in the spanwise direction [20]. The operators $\boldsymbol{M}$ and $\mathcal{L}$ are made invertible via enforcement of the boundary conditions; in the velocity/vorticity formulation, this corresponds to $\hat{v} = \frac{\partial \hat{v}}{\partial y} = \hat{\eta} = 0$ at the walls.

The corresponding mean-momentum equations which govern $\mathbf{U}(y,z)$ are given by

$$\begin{cases} VU_y + WU_z + \frac{\partial \langle p\rangle}{\partial x} - \frac{1}{Re}\left(U_{yy} + U_{zz}\right) = \langle f_u\rangle \\ VV_y + WV_z + \frac{\partial \langle p\rangle}{\partial y} - \frac{1}{Re}\left(V_{yy} + V_{zz}\right) = \langle f_v\rangle \\ VW_y + WW_z + \frac{\partial \langle p\rangle}{\partial z} - \frac{1}{Re}\left(W_{yy} + W_{zz}\right) = \langle f_w\rangle \\ V_y + W_z = 0. \end{cases} \tag{13}$$

Notably, the equations for V and W are decoupled from U. From the continuity equation, we can define the stream-function $\Lambda(y,z)$ [11, 12] such that

$$V = -\Lambda_z, \;\; W = \Lambda_y. \tag{14}$$

Consequently, upon differentiating the V-momentum with respect to z and the W-momentum with respect to y and subtracting the two, we can recast equation 13 as

$$\begin{cases} \Lambda_z\left[\Lambda_{yyy} + \Lambda_{yzz}\right] - \Lambda_y\left[\Lambda_{zzz} + \Lambda_{yyz}\right] + \frac{1}{Re}\left[\Lambda_{yyyy} + \Lambda_{zzzz} + 2\Lambda_{yyzz}\right] = \langle f_v\rangle_z - \langle f_w\rangle_y \\ -\Lambda_z U_y + \Lambda_y U_z + \frac{\partial \langle p\rangle}{\partial x} - \frac{1}{Re}\left(U_{yy} + U_{zz}\right) = \langle f_u\rangle. \end{cases} \tag{15}$$

Thus, the solution to the mean-momentum equations amounts to first solving a nonlinear equation for $\Lambda(y,z)$ and using this result to solve a linear equation for U. In discretized form (Chebyshev/Fourier), the equation for Λ yields a system of nonlinear algebraic equations and is solved for iteratively using the MATLAB function *fsolve* with an initial guess of $\Lambda = 0$. In the case of Couette flow, $\frac{\partial \langle p\rangle}{\partial x} = 0$. For Poiseuille flow, $\frac{\partial \langle p\rangle}{\partial x}$ is adjusted to enforce a prescribed mass flux, here taken as $Q = 4/3$.

B. A low-dimensional iterative scheme

Returning our attention to the resolvent operator, there are many instances in which the operator is inherently low-dimensional and linear tools can be leveraged to exploit this property. Specifically, a singular value decomposition (SVD) of $\mathcal{H}(k_x,\omega)$ yields

$$\mathcal{H}(k_x,\omega) = \Psi\Sigma\Phi^H, \tag{16}$$

where Ψ contains an ordered set of response modes $\hat{\boldsymbol{\psi}}_i(y,z)$, Φ contains an ordered set of forcing modes $\hat{\boldsymbol{\phi}}_i(y,z)$, and Σ is a diagonal matrix containing the singular values σ_i representing the gain between forcing and response. When the operator is low-rank, i.e. $\sigma_1 \gg \sigma_2$, we can express, often to a good approximation, the velocity field as

$$\hat{\mathbf{u}}(k_x,\omega) \approx A\hat{\boldsymbol{\psi}}_1(y,z), \tag{17}$$

where $A = \sigma_1\chi_1$ and the weight $\chi_1 = \langle \hat{\mathbf{f}}, \hat{\boldsymbol{\phi}}_1\rangle$ is the projection of the nonlinear forcing onto the leading forcing mode. It has been demonstrated for several of the lower branch ECS in channels [21] that the approximation in equation 17 is a very accurate representation when evaluated at the fundamental streamwise wavenumber $k_{x_f} = \frac{2\pi}{L_x}$ and corresponding frequency $\omega = ck_{x_f}$, where c is the wavespeed of the solution. This low-rank behavior can be attributed to, as will be demonstrated more rigorously in the following section, the (near) neutral stability of the

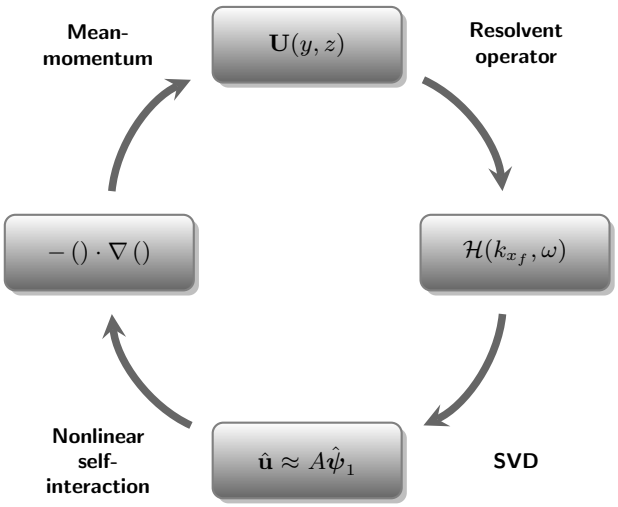

FIG. 1: An adaptation of the self-sustaining process [5] used to iteratively compute ECS. An initial laminar velocity profile serves as an input to the resolvent operator. The leading singular mode of the operator provides an approximation of the streamwise-varying field; the nonlinear self-interaction is computed and used to generate a new mean velocity field $\mathbf{U}(y,z)$. The loop is repeated until $\mathbf{U}(y,z)$ not only converges, but also yields a resolvent operator that is high-gain (i.e. $\sigma_1 \gg 1$) and sufficiently low-rank (i.e. $\sigma_1 \gg \sigma_2$). The latter two conditions serve as a proxy for the neutral stability of $\mathbf{U}(y,z)$. For a fixed box size and Reynolds number, the loop requires the specification of only two unknown parameters: the wavespeed $c = \omega/k_{x_f}$ and the amplitude A of the streamwise-varying mode.

mean $\mathbf{U}(y,z)$ which effectively creates a resonance condition at the frequency $\omega = ck_{x_f}$. In this case, the resolvent norm is inversely proportional to the distance to the nearest eigenvalue [22]; in the strict limit of a neutrally-stable eigenvalue, the resolvent operator would be singular. Furthermore, the Reynolds stresses generated by the single streamwise-varying Fourier mode are enough to sustain the mean, completing the self-sustaining process as outlined by [5]. Thus, from the resolvent-based perspective of equation 17, with knowledge of $\mathbf{U}(y,z)$ we can effectively close the system. The only unknown is the weight χ_1 which can be computed with a weakly-nonlinear type analysis [23].

However, in general, *a priori* knowledge of $\mathbf{U}(y,z)$ can be considered a very limiting assumption. Here, we wish to utilize the aforementioned framework but starting from simpler origins. Specifically, we wish to demonstrate if progress can be made starting from an initial laminar profile. We propose an iterative procedure as illustrated in Figure 1. We use the initial laminar profile ($\mathbf{U}(y,z) = y\hat{\mathbf{i}}$, $\mathbf{U}(y,z) = (1-y^2)\hat{\mathbf{i}}$ for Couette and Poiseuille flows respectively, where $\hat{\mathbf{i}}$ is a unit vector in the streamwise direction) as an input to the resolvent operator. Using equation 17, the fluctuating velocity field is approximated by the leading singular mode of the resolvent operator. The nonlinear self-interaction is computed and fed into the right-hand side of equation 15, which is solved to provide an updated mean velocity input. The procedure is then repeated until three conditions are met: (i) the cycle self-sustains (i.e. $\mathbf{U}(y,z)$ converges), (ii) the low-rank approximation of equation 17 is valid, and (iii) $\mathbf{U}(y,z)$ is (nearly) neutrally stable. The latter two conditions are monitored by analyzing the signature of the singular values of the resolvent operator. Whether these three conditions is met is dependent on the selection of the two unknown parameters in the model: the wavespeed c and amplitude A (we emphasize that while in general A is complex, since we are considering a single streamwise-varying Fourier mode we need only specify the magnitude of A). Stated more precisely, for a fixed box size and Reynolds number, we seek values of A and c such that

$$\begin{cases} \dfrac{\left\|\mathbf{U}^{j+1}(y,z) - \mathbf{U}^{j}(y,z)\right\|_2}{\left\|\mathbf{U}^{j}(y,z)\right\|_2} \leq \epsilon \\ \dfrac{\sigma_1}{\sigma_2} \geq \gamma \\ \sigma_1 \geq \sigma_c \end{cases} \tag{18}$$

for some threshold values ϵ, γ, and σ_c, where $j = 0, 1, 2, ...$ is the iteration index, $\mathbf{U}^0(y,z)$ is the laminar profile, and $\|\ \|_2$ denotes the L^2-norm. For what follows, we choose values of $\epsilon = 0.01$, $\gamma = 10$, and $\sigma_c = 1000$ though significant sensitivity to these values was not observed. It was found that fixing values for A and c at iteration $j = 0$ more reliably lead to convergence. The wavespeeds considered ranged from zero to the maximum velocity of the laminar profile.

An upper bound for the amplitude A could be approximated by finding a critical value such that the computation of the streamfunction Λ during the initial iteration failed to converge. With only two parameters, a sweep could be performed to find candidate values in a manner that was computationally tractable. Inaccuracies in the true values of A and c of approximately ten and five percent respectively still lead to converged solutions, suggesting a certain level of robustness to the algorithm.

III. RESULTS

We consider the same domain sizes of [24] and [4] to compute ECS in Couette and Poiseuille flows and, in this particular study, seek solutions for the two flows for $Re = 1000$ and $Re = 3000$ respectively. This choice of domain and Reynolds number was selected to facilitate comparisons to previous studies. A summary of the relevant geometrical and flow parameters are found in Table I. With the box size and Reynolds number established, we can proceed with the algorithm illustrated in Figure 1.

TABLE I: Summary of relevant flow and geometrical parameters.

Flow	L_x	L_z	N_x	N_y	N_z	Re	c	A
Couette	$2\pi/1.14$	$2\pi/2.5$	32	35	32	1000	0	0.02
Poiseuille	π	$\pi/2$	24	81	24	3000	0.88	0.009

In Figure 2, we show the results of the iterative approach for Couette flow with wavespeed of $c = 0$ and amplitude $A = 0.02$. We plot the magnitude of the $\hat{u}$, $\hat{v}$, and $\hat{w}$ components of the fundamental streamwise Fourier mode, along with the resulting mean velocity field (deviation from laminar). The first three columns show the first three iterations respectively, with the third iteration satisfying the criterion outlined in equation 18. To verify if this is indeed a potential solution, we write the velocity field in the form

$$\mathbf{u}(x, y, z) = \mathbf{U}(y, z) + \left(A\hat{\boldsymbol{\psi}}_1 e^{ik_{x_f} x} + c.c. \right) \tag{19}$$

where c.c. denotes complex conjugate, and input this field to the Newton-Krylov-hookstep solver implemented in Channelflow [25]. While we only specify the mean and fundamental streamwise Fourier modes, we use the streamwise resolution as shown in Table I to match previous studies and ensure proper convergence of the solution. This guess quickly converges to an ECS solution, as plotted in the last column of Figure 2, needing only three Newton iterations to achieve a relative error of $\mathcal{O}(10^{-13})$. Thus, the field from the third iteration provides an excellent approximation; the relative difference between this field and the true solution with respect to an L^2-norm is $\approx 0.7\%$. In addition, for the plots of the converged solution, we show the location of the corresponding critical layer $U(y, z) = c = 0$. As is the case with most lower branch solutions, the fluctuations are localized around this location. It should be noted this particular ECS has been previously computed and reported for $Re = 400$ by [24] (and labeled as EQ7), though not by this methodology.

In a similar manner, the results for Poiseuille flow with choices of $c = 0.88$ and $A = 0.009$ are found in Figure 3. We plot the same fields as in Figure 2, but with the first three columns representing the first, second, and fifth iterations respectively and the last column showing the converged solution obtained from Channelflow (requiring four Newton iterations). We again observe a close correspondence between the final iteration and the true solution (relative error of 1.4%), as well as localization of the fluctuations around the critical layer $U(y, z) = c = 0.88$. To the authors' knowledge, this solution has not been previously reported. Though we do not show it here, a second traveling wave solution was also found using this iterative method for values of $c = 0.69$ and $A = 0.01$, suggesting multiple solutions can be computed for a fixed Reynolds number and box size using this approach.

In order to validate the notion of the (near) neutral stability of the ECS mean fields, we plot the corresponding eigenvalues of the linearized Navier-Stokes operator $\mathcal{L}_1$ associated with $\mathbf{U}(y, z)$ (for the converged solution) and evaluated at $k_x = k_{x_f}$, as seen in Figure 4. The same computation was performed on a higher-resolution grid to ensure proper convergence of the eigenvalues. We also plot σ_1 and σ_2 (black and green lines, respectively) as a function of wavespeed for the two flows. We observe the presence of an approximately neutrally stable eigenvalue for each flow, as indicated by the red circles located at the wavespeed of the respective solutions. Consequently, we see a near-resonance response in the singular values, with $\sigma_1 \gg 1$ and $\sigma_1 \gg \sigma_2$ when evaluated at the wavespeed. It is worth remarking that these associated eigenvalues lie, albeit barely, in the unstable right-half plane (the growth rates are $\mathcal{O}(10^{-3})$). In general, this would invalidate a resolvent analysis as these disturbances would grow in time and would not yield a stationary mean flow. However, in a practical numerical sense for ECS, we consider the growth rates

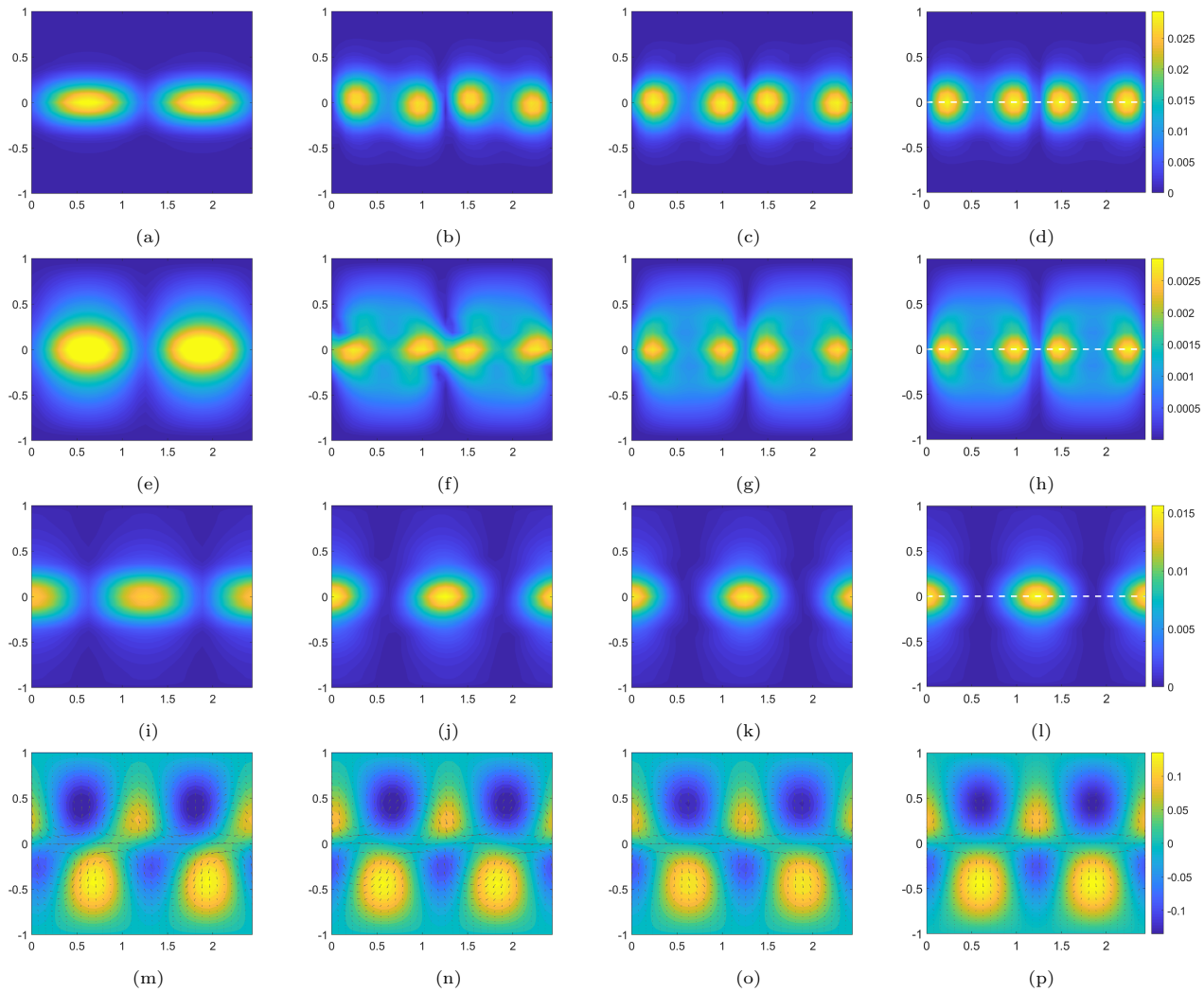

FIG. 2: Couette flow: The amplitude as a function of spanwise (horizontal axis) and wall-normal (vertical axis) distance of the (a)-(d) u-component, (e)-(h) v-component, and (i)-(l) w-component of the fundamental streamwise Fourier mode k_{x_f} along with the (m)-(p) resulting mean velocity $\mathbf{U}(y,z)$ (shown as the deviation from laminar) generated from the self-interaction of the single Fourier mode. The first three columns represent the first three iterations respectively for an initial laminar profile, and the last column shows the converged field computed using Channelflow with iteration 3 as an input. The white dashed line in the last column designates the location of the critical layer, $U(y,z)=0$. This solution was previously computed by [24] and designated as EQ7.

sufficiently small to be regarded as effectively neutrally stable. Though not reported here, additional computations suggest this growth rate continues to decrease for increasing Reynolds number. This is consistent with the high-Reynolds number asymptotic results of [8], in which the flow is properly described by a single streamwise varying mode; at this moderate Reynolds number, we are clearly approaching, though with small numerical discrepancy, this asymptotic behavior. In this instance, we also note that the corresponding eigenvectors are identical in structure to the leading resolvent modes [26]. The fact that the eigenvalues and eigenvectors associated with the mean can correctly identify the wavespeed and spatial structure is again consistent with other studies in which a linearization about the mean flow was performed. In particular, due to the dominance of the single streamwise varying mode, the associated nonlinear contributions from higher wavenumbers is negligibly small and equation 5 yields (setting the right-hand side to zero) the associated eigenvalue problem, as argued by [19]. However, at least with regards to the iterative algorithm used herein where the initial laminar field is not neutrally stable, it was observed that use of the singular modes of the resolvent operator, as opposed to the eigenvectors of the linearized operator, more robustly led to convergence of solutions.

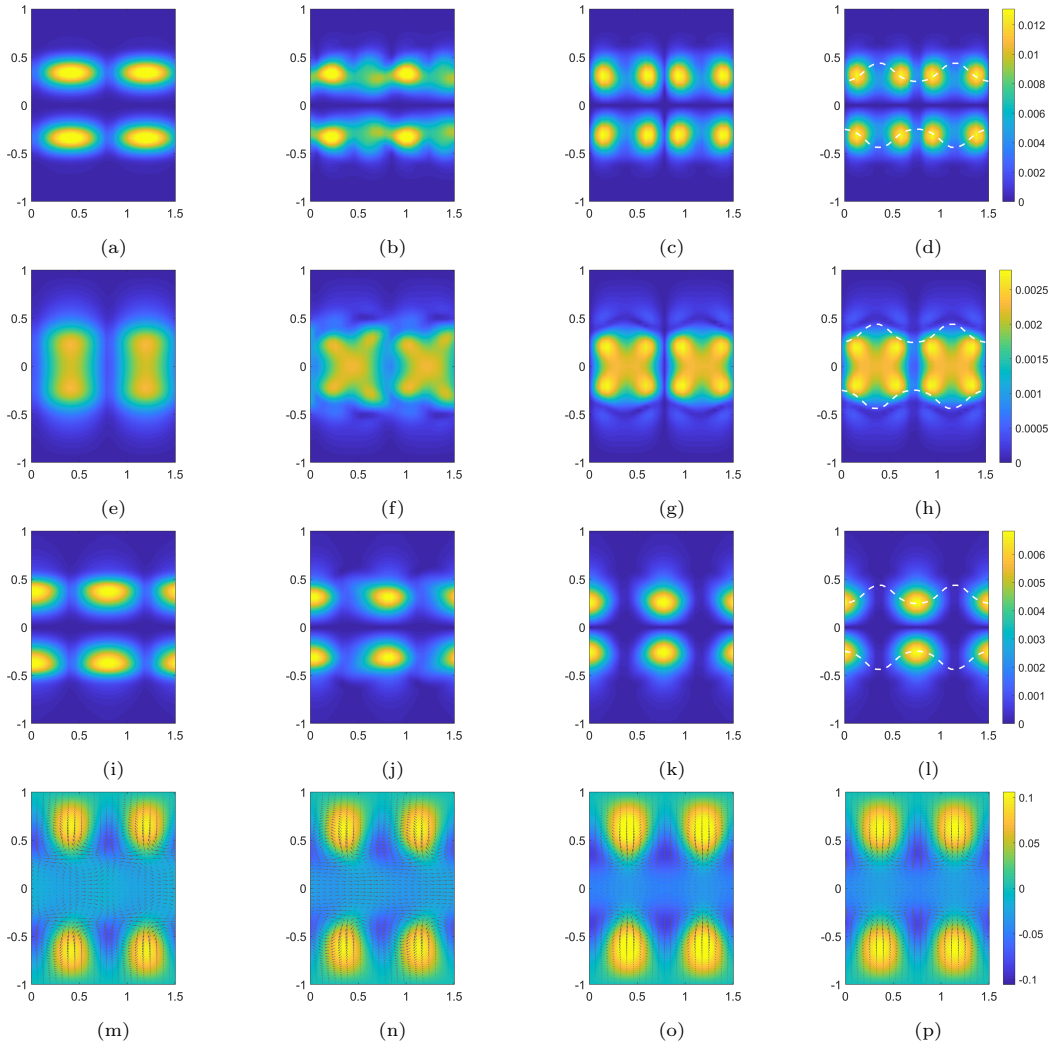

FIG. 3: Poiseuille flow: The amplitude as a function of spanwise (horizontal axis) and wall-normal (vertical axis) distance of the (a)-(d) u-component, (e)-(h) v-component, and (i)-(l) w-component of the fundamental streamwise Fourier mode k_{x_f} along with the (m)-(p) resulting mean velocity $\mathbf{U}(y,z)$ (shown as the deviation from laminar) generated from the self-interaction of the single Fourier mode. The first three columns represent the first, second, and fifth iterations respectively for an initial laminar profile, and the last column shows the converged field computed using Channelflow with iteration 5 as an input. The white dashed line in the last column designates the location of the critical layer, $U(y,z) = c = 0.88$.

IV. CONCLUSION

We have presented a low-order, resolvent-based method to compute ECS in channels. We demonstrated, starting from an initial laminar profile, an iterative procedure to compute traveling wave solutions in Couette and Poiseuille flow requiring the specification of only two unknown parameters, namely the wavespeed and amplitude of a single streamwise-varying Fourier mode. The low-dimensionality of the approach leverages the properties of the resolvent operator for the underlying (nearly) neutrally stable (streamwise-averaged) mean flow and perhaps suggests that (lower-branch) solutions of the Navier-Stokes equation can be described in extraordinarily simple forms.

The framework is quite general in its formulation; it would be worthwhile to utilize this approach for other shear flows such as boundary layers and pipe flow. In addition to starting from a laminar solution, simple analytic expressions for the mean forcing may be useful to generate an initial roll/streak mean flow, as explored by [5] and [8]. A potential improvement to the current formulation would be to incorporate an optimization step to more directly drive the mean flow towards a neutrally stable configuration. While the current approach seems only applicable to lower-branch states at these moderate Reynolds numbers, there is evidence these ideas can be extended to upper-branch states, though

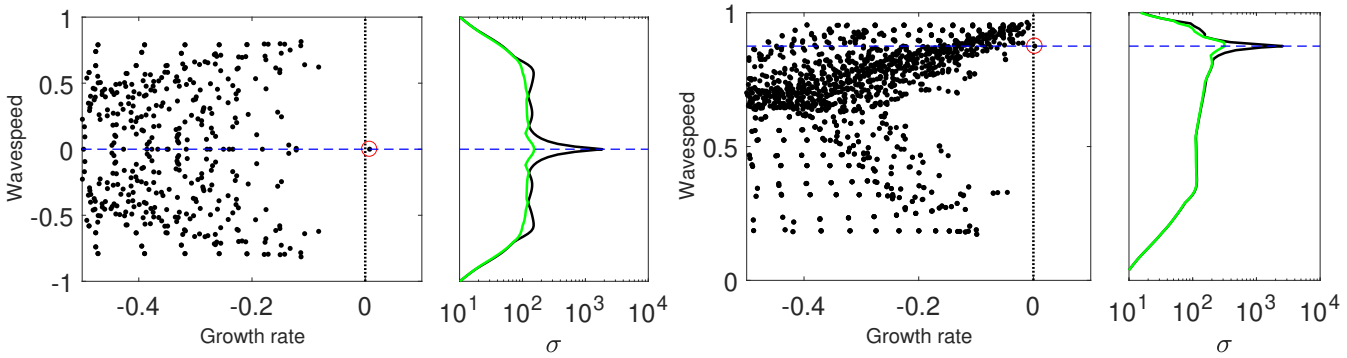

FIG. 4: Eigenvalues (dots) of the linearized Navier-Stokes operator associated with the 2D/3C mean $\mathcal{L}_1$ evaluated at k_{x_f}, and the first two singular values as a function of wavespeed (black and green lines, respectively) of the (a) Couette and (b) Poiseuille ECS solutions. We note the presence of a nearly neutrally stable eigenvalue (red circles) and hence large resolvent norm for the respective wavespeeds of $c = 0$ and $c = 0.88$ of the solutions (dashed blue line).

at higher Reynolds numbers [27], and is a subject of future work; however, flows with more than one energetically significant streamwise-varying mode would require more sophisticated modeling efforts. We wish to eventually extend this methodology to the computation of periodic orbits as well. Ultimately, we hope the results presented herein will inform the continued efforts to model turbulence using the 2D/3C framework, particularly by augmenting them with frequency-based input/output techniques.

Appendix

The block operators in equation 8, i.e. the Orr-Sommerfeld, Squire, and coupling operators for a 2D/3C mean, are defined below. These operators have previously been defined in [12] and [22] where terms involving Λ have been neglected.

$$\begin{aligned}\mathcal{L}_{OS} = {} & ik_xU\Delta + ik_xU_{zz} + 2ik_xU_z\partial_z - ik_xU_{yy} + 2ik_xU_z\partial^3_{yyz}\Delta_2^{-1} + 2ik_xU_{yz}\partial^2_{yz}\Delta_2^{-1} \\ & - \frac{1}{Re}\Delta^2 - (\Lambda_{yyz} + \Lambda_{zzz})\,\partial_y + 2\,(\Lambda_{yyz} + \Lambda_{zzz})\,\partial^3_{yzz}\Delta_2^{-1} - (\Lambda_{yyy} + \Lambda_{yzz})\,\partial_z \\ & - 2\Lambda_{zz}\partial^3_{yyz}\Delta_2^{-1} + 2\Lambda_{yz}\partial^3_{yzz}\Delta_2^{-1} - \Lambda_z\Delta\partial_y - 2\Lambda_{zz}\partial^2_{yz} - \Lambda_{yyyz} - \Lambda_{yzzz} - \Lambda_{yz}\Delta \\ & + \Lambda_{yyy}\partial_z\Delta + 2\Lambda_{yz}\partial^2_{zz} + \Lambda_{yyzz}\partial^2_{yz}\Delta_2^{-1} + \Lambda_{zzzz}\partial^2_{yz}\Delta_2^{-1} + \Lambda_{zz}\partial^2_{yz}\Delta\Delta_2^{-1}\end{aligned} \tag{A.1}$$

$$\begin{aligned}\mathcal{L}_{C_1} = {} & -2k_x^2U_z\partial_y\Delta_2^{-1} - 2k_x^2U_{yz}\Delta_2^{-1} + 2ik_x\,(\Lambda_{yyz} + \Lambda_{zzz})\,\partial_z\Delta_2^{-1} - 2ik_x\Lambda_{zz}\partial^2_{yy}\Delta_2^{-1} \\ & + 2ik_x\Lambda_{yz}\partial^2_{yz}\Delta_2^{-1} + ik_x\Lambda_{yyzz}\Delta_2^{-1} + ik_x\Lambda_{zzzz}\Delta_2^{-1} + ik_x\Lambda_{zz}\Delta\Delta_2^{-1}\end{aligned} \tag{A.2}$$

$$\mathcal{L}_{C_2} = -U_z\partial_y + U_{yz} + U_y\partial_z - U_{zz}\partial^2_{yz}\Delta_2^{-1} + ik_x\Lambda_{yyzz}\partial^2_{yy}\Delta_2^{-1} \tag{A.3}$$

$$\mathcal{L}_{SQ} = ik_xU - ik_xU_{zz}\Delta_2^{-1} + \Lambda_{yz} - \Lambda_z\partial_y + \Lambda_y\partial_z - \Lambda_{zz}\partial^2_{yz}\Delta_2^{-1} - \frac{1}{Re}\Delta \tag{A.4}$$

ACKNOWLEDGMENTS

The support of ONR under Grant No. N00014-17-1-2307 and AFOSR under Grant No. FA 9550-16-1-0361 is gratefully acknowledged.

[1] G. Kawahara, M. Uhlmann, and L. Van Veen, The significance of simple invariant solutions in turbulent flows, Annu. Rev. Fluid Mech. **44**, 203 (2012).

[2] J. F. Gibson, J. Halcrow, and P. Cvitanović, Visualizing the geometry of state space in plane Couette flow, J. Fluid Mech. **611**, 107 (2008).

[3] N. Budanur and B. Hof, Complexity of the laminar-turbulent boundary in pipe flow, Phys. Rev. Fluids **3**, 054401 (2018).

[4] J. S. Park and M. D. Graham, Exact coherent states and connections to turbulent dynamics in minimal channel flow, J. Fluid Mech. **782**, 430 (2015).

[5] F. Waleffe, On a self-sustaining process in shear flows, Phys. Fluids **9**, 883 (1997).

[6] S. C. Reddy, P. J. Schmid, J. S. Baggett, and D. S. Henningson, On stability of streamwise streaks and transition thresholds in plane channel flows, J. Fluid Mech. **365**, 269 (1998).

[7] P. Schmid and D. Henningson, *Stability and Transition in Shear Flows*, Vol. 142 (Springer Science & Business Media, 2000).

[8] P. Hall and S. Sherwin, Streamwise vortices in shear flows: harbingers of transition and the skeleton of coherent structures, J. Fluid Mech. **661**, 178 (2010).

[9] V. Mantič-Lugo, C. Arratia, and F. Gallaire, Self-consistent mean flow description of the nonlinear saturation of the vortex shedding in the cylinder wake, Phys. Rev. Lett. **113**, 084501 (2014).

[10] K. M. Bobba, *Robust flow stability: theory, computations and experiments in near wall turbulence*, Ph.D. thesis, California Institute of Technology (2004).

[11] D. F. Gayme, B. J. McKeon, A. Papachristodoulou, B. Bamieh, and J. C. Doyle, A streamwise constant model of turbulence in plane Couette flow, J. Fluid Mech. **665**, 99 (2010).

[12] B. F. Farrell and P. J. Ioannou, Dynamics of streamwise rolls and streaks in turbulent wall-bounded shear flow, J. Fluid Mech. **708**, 149 (2012).

[13] V. L. Thomas, B. F. Farrell, P. J. Ioannou, and D. F. Gayme, A minimal model of self-sustaining turbulence, Phys. Fluids **27**, 105104 (2015).

[14] M. Pausch, Q. Yang, Y. Hwang, and B. Eckhardt, Quasilinear approximation for exact coherent states in parallel shear flows, Fluid Dyn. Res. (2018).

[15] F. Alizard and D. Biau, Restricted nonlinear model for high-and low-drag events in plane channel flow, J. Fluid Mech. **864**, 221 (2019).

[16] A. S. Sharma, R. Moarref, B. J. McKeon, J. S. Park, M. D. Graham, and A. P. Willis, Low-dimensional representations of exact coherent states of the Navier-Stokes equations from the resolvent model of wall turbulence, Phys. Rev. E **93**, 021102 (2016).

[17] K. Rosenberg and B. J. McKeon, Efficient representation of exact coherent states of the Navier-Stokes equations using resolvent analysis, Fluid Dyn. Res. **51**, 011401 (2019).

[18] D. Barkley, Linear analysis of the cylinder wake mean flow, Europhys. Lett. **75**, 750 (2006).

[19] S. Turton, L. Tuckerman, and D. Barkley, Prediction of frequencies in thermosolutal convection from mean flows, Phys. Rev. E **91**, 043009 (2015).

[20] J. A. Weideman and S. C. Reddy, A MATLAB differentiation matrix suite, ACM Trans. Math. Softw. **26**, 465 (2000).

[21] K. Rosenberg, *Resolvent-based modeling of flows in a channel*, Ph.D. thesis, California Institute of Technology (2018).

[22] P. J. Schmid and D. S. Henningson, *Stability and transition in shear flows* (Springer, 2001).

[23] K. Rosenberg, S. Symon, and B. J. McKeon, Role of parasitic modes in nonlinear closure via the resolvent feedback loop, Phys. Rev. Fluids **4**, 052601 (2019).

[24] J. F. Gibson, J. Halcrow, and P. Cvitanović, Equilibrium and travelling-wave solutions of plane Couette flow, J. Fluid Mech. **638**, 243 (2009).

[25] J. F. Gibson, Channelflow: a spectral Navier-Stokes simulator in C++, University of New Hampshire (2012).

[26] S. Symon, K. Rosenberg, S. Dawson, and B. J. McKeon, Non-normality and classification of amplification mechanisms in stability and resolvent analysis, Phys. Rev. Fluids **3**, 053902 (2018).

[27] K. Deguchi and P. Hall, The high-Reynolds-number asymptotic development of nonlinear equilibrium states in plane Couette flow, J. Fluid Mech. **750**, 99 (2014).